



## Scaled-up 2D solid-state laser array

NIHUI ZHANG,<sup>1,2,†</sup> ZHENJIAO SHAN,<sup>3,†</sup> FANSHENG MENG,<sup>1,3</sup> DI XIN,<sup>4,5</sup> HAI WANG,<sup>1,2</sup> TING FU,<sup>5</sup> AIYI QI,<sup>1,2,6</sup> HONGWEI QU,<sup>1,2,6</sup> XUYAN ZHOU,<sup>1,2,6</sup> WANHUA ZHENG,<sup>1,2,6,7</sup> AND HONGBO ZHANG<sup>3,\*</sup>

<sup>1</sup>The Laboratory of Solid State Optoelectronics Information Technology, Institute of Semiconductors, Chinese Academy of Sciences, Beijing 100083, China

<sup>2</sup>The Center of Materials Science and Optoelectronics Engineering, University of Chinese Academy of Sciences, Beijing 101408, China

<sup>3</sup>The School of Optoelectronics, University of Chinese Academy of Sciences, Beijing 101408, China

<sup>4</sup>The School of Physics and Physical Engineering, Qufu Normal University, Jining 273165, China

<sup>5</sup>The Weifang Academy of Advanced Opto-Electronic Circuits, Weifang 261000, China

<sup>6</sup>The State Key Laboratory on Integrated Optoelectronics, Institute of Semiconductors, Chinese Academy of Sciences, Beijing 100083, China

<sup>7</sup>whzheng@semi.ac.cn

<sup>†</sup>These authors contributed equally to this work.

\*hbzhang@ucas.ac.cn

Received 6 January 2025; revised 16 March 2025; accepted 18 March 2025; posted 18 March 2025; published 11 April 2025

**The inherent trade-off between high-power and high beam quality has long been a critical technological challenge for high-power vertical-cavity surface-emitting lasers (VCSELs), fundamentally limiting their direct application, especially in remote large area irradiation and detection. Here, a compact and efficient two-dimensional (2D) laser array based on a vertical-cavity surface-emitting laser (VCSEL) array is proposed and demonstrated. By employing a highly doped Nd:YVO<sub>4</sub> crystal and a specialized cavity to compensate thermal lensing effect, the laser array achieves a 1 μm wavelength, 4.7 mJ pulse energy, 52% optical-to-optical (O-O) conversion efficiency, and a brightness of 1.27 kW·cm<sup>-2</sup>·sr<sup>-1</sup>, which is three orders higher than that of the 808 nm VCSEL array (5.9 W·cm<sup>-2</sup>·sr<sup>-1</sup>). The beam quality factors (M<sup>2</sup>) of individual emitters were 1.41 and 1.48 in the X and Y directions, respectively. Additionally, the laser power scales with the array size, demonstrating the potential for innovative photonics applications.** © 2025 Optica Publishing Group. All rights, including for text and data mining (TDM), Artificial Intelligence (AI) training, and similar technologies, are reserved.

<https://doi.org/10.1364/OL.554966>

Solid-state lasers are pivotal in both fundamental research and technological applications and have been extensively used in high-precision material processing, free-space light communication, laser cooling, light tweezers, and the development of laser weapons [1–6]. However, their large capacity, high cost, and reliance on powerful pump sources strictly limit their scalability and adoption in compact applications, despite the advantages of excellent beam quality and stability. The miniaturization and integration of solid-state lasers have become vital for advancing laser technology, with recent progress driven by photonic integration and microelectromechanical systems (MEMS) technologies [7,8]. These advancements enable the incorporation of pump sources, laser gain materials, and light components

onto microchip platforms; moreover, compact devices suited for portable and embedded systems have been created [9,10]. However, challenges remain in terms of heat dissipation, maintaining efficiency on miniaturized platforms, and overcoming integration and material limitations. Vertical-cavity surface-emitting lasers (VCSELs) are ideal candidates as pump sources for solid-state lasers because of their excellent beam circularity, easy beam shaping, insensitivity to wavelength variations, integrability, and expansibility [11,12]. Efforts on VCSEL-pumped solid-state lasers are ongoing [13–16]. High-power VCSEL end-pumping of solid-state lasers typically involves the utilization of a lens system to focus the beam and inject it into the crystal. However, the high pumping density induces significant thermal effects, which ultimately constrain the scalability of solid-state lasers, although increasing the active layer thickness and oxide aperture in VCSELs can enhance high-power output. However, such enlargement inevitably induces higher-order modes in both vertical and transverse directions, significantly degrading beam quality and consequently reducing brightness [17]. This trade-off between high-power and high beam quality has long been a critical technological challenge for high-power VCSELs, fundamentally limiting their direct application. As a result, achieving high-brightness, high-power surface-emitting lasers remains a central challenge in the field.

In this paper, we originally developed an efficient scaled-up 2D solid-state laser array that directly combined large-scale VCSEL arrays with a laser crystal. This array system is capable of simultaneously emitting thousands of laser beams while achieving effective light mode coupling and optimized thermal management. The 2D laser array also evidently has high brightness and the ability to scale with the array size. A specially designed oscillation cavity paired with a 1 at.% Nd:YVO<sub>4</sub> crystal was used to mitigate thermal lensing. Integration of the laser array produced a pulse energy of 4.7 mJ at a wavelength of 1 μm, achieving an O-O efficiency of 52%. The resulting brightness was 1.27 kW·cm<sup>-2</sup>·sr<sup>-1</sup>; this value represented a three-order-of-magnitude enhancement compared with that of

the VCSEL array ( $5.9 \text{ W}\cdot\text{cm}^{-2}\cdot\text{sr}^{-1}$ ). The measured beam quality factors ( $M^2$ ) of individual laser emitters in the array were 1.41 and 1.48 along the X and Y directions, respectively. These values indicated the high-quality beam properties across the laser array. Additionally, a comparison of the laser outputs from the  $1 \times 1 \text{ mm}^2$  and  $3 \times 3 \text{ mm}^2$  arrays revealed that the power increased proportionately with the size of the laser array.

The light platform fabrication concept for a scaled-up 2D solid-state laser array pumped by an 808 nm VCSEL array is illustrated in Fig. 1(a). The copper heat sink utilized fin-integrated 400  $\mu\text{m}$  wide microchannels and cooled with deionized water. The 1 at.% Nd:YVO<sub>4</sub> crystal was adhered to the VCSEL array via the glue bonding technique. Two film-coated surfaces of the Nd:YVO<sub>4</sub> crystal constructed a resonant cavity. The arrayed VCSEL emitter pumping resulted in the formation of a highly integrated 2D solid-state laser array. We first assessed the light field characteristics of the VCSEL array. Importantly, the  $1 \times 1 \text{ mm}^2$  and  $3 \times 3 \text{ mm}^2$  VCSEL arrays exhibited no fundamental differences in structural design. Key parameters, such as the oxide aperture diameter and the mesa center-to-center distance, were consistent for the two arrays. Figure 1(b) shows the layout of the  $3 \times 3 \text{ mm}^2$  VCSEL array. The structure of the  $3 \times 3 \text{ mm}^2$  VCSEL array was designed for top emission. The  $3 \times 3 \text{ mm}^2$  VCSEL array consisted of a  $54 \times 62$  emitter pixel matrix, totaling 3348 emitters, and each had an oxide aperture diameter of 12  $\mu\text{m}$ . The mesa diameter was 42  $\mu\text{m}$ , with a center-to-center pitch of 48  $\mu\text{m}$ . The divergence angle of each VCSEL emitter was measured to be  $30^\circ$ . The VCSEL array featured a three-sided current injection scheme and is shown in Fig. 1(c). The surface electrode consists of an annular electrode (inner radius, 10  $\mu\text{m}$ ; outer radius, 19  $\mu\text{m}$ ) and an aperture electrode (opening radius, 8  $\mu\text{m}$ ). The p-type electrode was bonded to the anode of the AlN heat sink using three-sided gold wire bonding, while the n-type electrode, on the VCSEL chip's backside, was soldered to the cathode via AuSn sintering. These electrodes were electrically isolated, ensuring device stability and reliable operation. Additionally, owing to the advantages of higher peak power and lower thermal effects than those of continuous-wave (CW) pumping, we employed a wide current pulse to drive the VCSEL array. Figure 1(d) shows the variation in the output energy with current at a pumping repetition frequency of 10 Hz and pulse width of 100  $\mu\text{s}$ . At a current of 100 A, the VCSEL array could output a maximum pulse energy of 9 mJ (Newport Corporation Brand, PE50BF-DIFH-C); this corresponded to a brightness of  $5.9 \text{ W}\cdot\text{cm}^{-2}\cdot\text{sr}^{-1}$ . As shown in Fig. 1(e), the linewidth of the emission spectrum of the VCSEL array was 0.7 nm at the full width at half maximum (FWHM) at the central wavelength of 808.56 nm (YOKOGAWA, AQ6370D). Figure 1(f) shows the near-field light image of the VCSEL array at 100 A is current driven. A partially enlarged image revealed that the beam profile and intensity distribution of each emitter in the array were consistent, indicating that the emitters exhibited similar emission characteristics.

An effective cavity design is crucial for compensating for thermal lensing to ensure alignment stability and uniformity in the laser array output. To assess the thermal lensing effect, a collimated He-Ne laser was directed at the Nd:YVO<sub>4</sub> crystal at a small angle. The crystal was affixed to the VCSEL array by applying adhesive along its edges (UV788-2 adhesive, provided by PENCHEM), followed by a curing process under ultraviolet light for a duration of 2 min (Fig. 2(a)). The diameter variation of the reflected beam from the VCSEL surface was monitored using

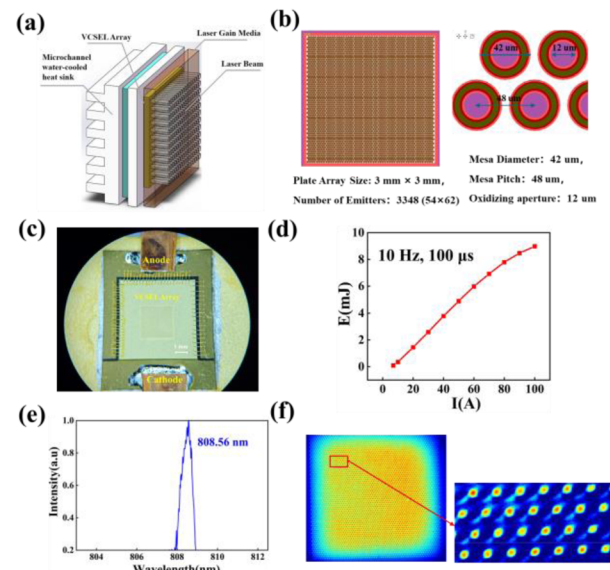


**Fig. 1.** (a) Schematic diagram of the 2D solid-state laser array. (b) Layout of the  $3 \times 3 \text{ mm}^2$  VCSEL array with 3,348 emitters, 42  $\mu\text{m}$  mesa size, 48  $\mu\text{m}$  mesa pitch, and 12  $\mu\text{m}$  oxidation aperture. (c) Photograph of the VCSEL array with a three-sided injection design for uniform current distribution. (d) Output energy versus current (10 Hz, 100  $\mu\text{s}$ ). (e) Emission spectrum with a central wavelength of 808.56 nm and an FWHM of 0.7 nm. (f) Near-field image and a partially enlarged image of the VCSEL array at an injection current of 100 A.

a laser beam profiler (LBP) (Coherent, LaserCam-HR II 1/2 in.). The thermal focal length induced by the Nd:YVO<sub>4</sub> crystal was determined by analyzing the focusing behavior of the reflected beam. Emitter distribution measurements were performed at a drive current of 100 A. Figure 2(b) shows a schematic of the experimental setup for the thermal lens characterization using a He-Ne laser. A collimating lens and LBP were employed to capture the beam profiles, and  $L_f$  denoted the distance between the VCSEL array and the LBP. In this setup,  $L_f$  was gradually set to 460 mm, 500 mm, and 540 mm to observe the beam profile variation. Figure 2(c) clearly shows the thermal lensing effect in the crystal and its influence on the luminous images of the VCSEL array illuminated by the He-Ne laser beam. The distribution characteristics of the localized array clearly reflected the manifestation of the thermal lens effect. Based on the lens combination formula, the focused beam measured at a distance of 500 mm indicated that the thermal focal length induced in the Nd:YVO<sub>4</sub> crystal was approximately 1000 mm.

To ensure beam stability within the laser cavity, effective compensation for the thermal lensing effect of the gain medium is essential. In the plano-concave resonator configuration, the focal length of the concave mirror matched the thermal focal length; compared with a plano-plano resonator, this configuration improved both the cavity stability and beam quality and provided superior performance. In the experiment, the surface of the Nd:YVO<sub>4</sub> crystal facing the VCSEL array was coated with a high-transmittance coating at 808 nm and a high-reflectance coating at 1064 nm, whereas the opposite surface was coated with a high-reflectance coating at 808 nm and a high-transmittance coating at 1064 nm. A plano-concave spherical mirror with a diameter of 6 mm was used as the

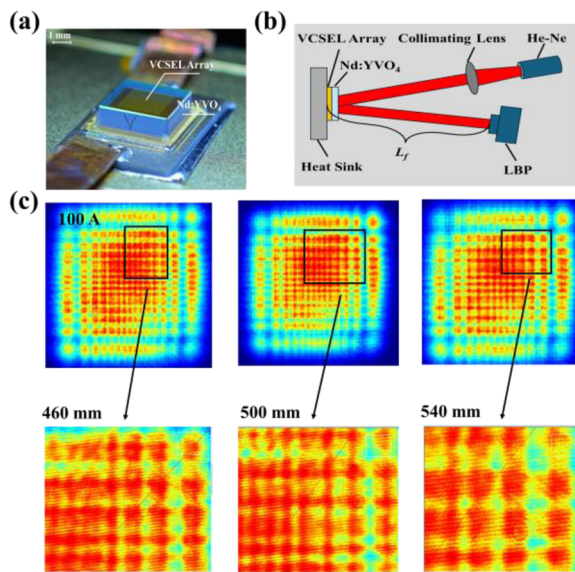


**Fig. 2.** (a) Photograph of the VCSEL array coupled with Nd:YVO<sub>4</sub> attached to its output facet by applying adhesive along the edges of the crystal. (b) Schematic diagram of the setup of the thermal lens measurement using a collimated He-Ne laser. (c) Luminous images of the VCSEL array at a drive current of 100 A, measured at distances of 460 mm, 500 mm, and 540 mm from the array, with partially enlarged views provided below.

output coupler (OC). The radius of curvature of the OC was 2000 mm. The concave surface of the OC was coated with a high-reflectivity coating at 808 nm and a partially transmissive coating at 1064 nm ( $T = 3\%$ ), whereas the planar surface was coated with high-transmittance coatings at both 808 nm and 1064 nm. The OC was mounted using a mechanical clamp and ensured direct contact between the concave surface and the Nd:YVO<sub>4</sub> crystal. As a result, the length of the laser cavity was equal to the thickness of the Nd:YVO<sub>4</sub> crystal, which was 1 mm. Figure 3(a) shows a photograph of the integrated 2D solid-state laser array. The plano-concave spherical mirror served as the OC and was held in place by a mechanical clamp. Figure 3(b) shows the curves of the laser output energy and O-O conversion efficiency versus the VCSEL pump energy at a repetition rate of 10 Hz. The system achieved an O-O conversion efficiency of 52% when the pump energy reached 9 mJ. Figure 3(c) shows the laser spectrum of the 2D solid-state laser array. The FWHM linewidth is 0.39 nm, with a central wavelength of 1064.39 nm. Figure 3(d) shows the near-field distribution of the laser beam emitter on the rear surface of the OC at a 52% O-O conversion efficiency. The laser emitter exhibited a distinct array distribution and had dimensions of approximately 3 mm in both directions of the array.

Based on the distribution characteristics of the 2D solid-state laser array shown in Fig. 3(d), a small aperture with a radius of 0.5 mm was used to extract a localized section from the central region of the array for more precise emitter positioning. The dimensions and inter-emitter pitch of neighboring emitters on the 2D solid-state laser array were measured. In Fig. 4(a), four adjacent emitters were selected, and their position coordinates were recorded. For each emitter, four coordinates (X1, X2, Y1, and Y2) were measured in millimeters. A comparison of these coordinates revealed that the sizes of the emitters were consistent, and each had a diameter of approximately

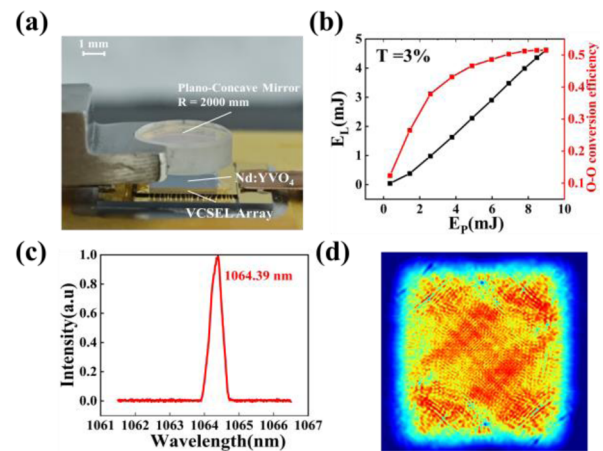


**Fig. 3.** (a) Photograph of the 2D solid-state laser array. The plano-concave OC mirror was held by a mechanical clamp. (b) Curve of the laser output energy and O-O conversion efficiency versus the VCSEL pump energy at a repetition rate of 10 Hz. (c) Laser spectrum of the 2D solid-state laser array. The FWHM linewidth of the spectrum is 0.39 nm, with a central wavelength of 1064.39 nm. (d) Near-field beam profile image of the 2D solid-state laser array.

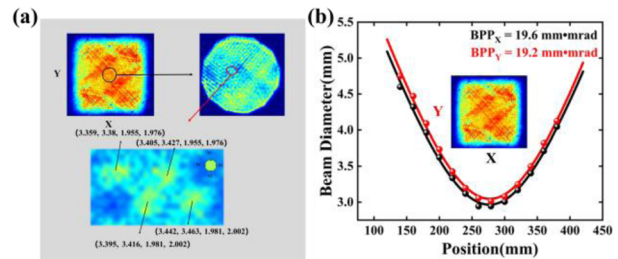


**Fig. 4.** (a) Process of characterizing the size of the emitters and the pitch between the emitters in the 2D solid laser array (inset: (X1, X2, Y1, and Y2) for each emitter coordinate). (b) At a drive current of 100 A, the laser beam sizes were 2.965 mm (X) and 3.0048 mm (Y), with half-divergence angles of 13.2 mrad and 12.8 mrad, respectively (inset: near-field beam profile of the 2D solid laser array).

22 μm and an inter-emitter pitch of approximately 46 μm. These results indicated that under VCSEL array pumping conditions, the individual emitters were capable of independently exciting the crystal. Distinct laser modes were formed in each excitation region, and minimal mutual interference occurred among the beams. Furthermore, the experimental results confirmed that the plano-concave resonator configuration effectively mitigated the excessive focusing caused by thermal lensing. This compensation mechanism alleviated the overconcentration of the laser beam within the Nd:YVO<sub>4</sub> gain medium, promoted a more uniform gain distribution, and maximized the overlap between the pump light and the laser mode field.

Figure 4(b) shows that at a drive current of 100 A, the laser beam from the array had an extent of 2.965 mm with a half-divergence angle of 13.2 mrad in the X direction. In the Y direction, the beam width was 3.0048 mm, with a half-divergence angle of 12.8 mrad. The inter-emitter pitch within the VCSEL array was on the order of micrometers, which minimized the impact of the emitter pitch on the beam overlap; thus, the impact of the emitter pitch was negligible. As a

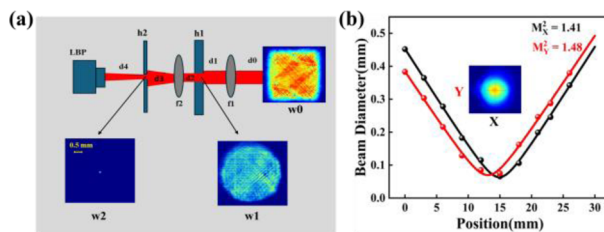


**Fig. 5.** (a) Beam quality testing setup for a single emitter at the center of the laser array. (b) Beam quality results for a single emitter (inset: beam profile at the beam waist).

result, the divergence angle of the VCSEL array was commonly considered approximately equal to that of the individual emitters [18]. Therefore, at an O–O conversion efficiency of 52%, the calculated brightness of the 2D solid-state laser array was  $1.27 \text{ kW}\cdot\text{cm}^{-2}\cdot\text{sr}^{-1}$ . This represented a three-order-of-magnitude increase in brightness compared with that of the VCSEL array ( $5.9 \text{ W}\cdot\text{cm}^{-2}\cdot\text{sr}^{-1}$ ). This increase in brightness highlights the significant potential of the 2D solid laser array for efficient energy conversion and applications. This array is particularly advantageous in fields requiring high brightness and energy density, such as precision machining, material processing, and high-power laser applications.

To further confirm that the emitted solid-state laser consisted of multiple independent beams and that each beam corresponded to an individual emitter in the VCSEL array, the setup shown in Fig. 5(a) was employed to measure the beam quality of a single emitter located at the center of the array. The beam quality factors for the single emitter were measured as  $M^2_x = 1.41$  and  $M^2_y = 1.48$  (Fig. 5(b)). Furthermore, experiments were conducted using a compact VCSEL array ( $1 \times 1 \text{ mm}^2$ , consisting of 288 emitters arranged in a  $16 \times 18$  configuration) as the pump source for the 2D solid-state laser array. At a pump energy of  $0.722 \text{ mJ}$  (8 A), the laser output energy was  $0.3 \text{ mJ}$ . A comparison with a  $3 \times 3 \text{ mm}^2$  2D solid-state laser array demonstrated that scaling up the array size resulted in a proportional increase in the laser output power. Additionally, the array architecture enabled the concurrent operation of multiple laser emitters on the same chip, thereby enhancing system integration and operational flexibility. This compact configuration not only enhanced the spatial efficiency but also reduced the production costs. The technology is scalable, and each laser emitter can be independently controlled; thus, the output performance is tunable and can be optimized to meet diverse application demands.

In this paper, highly doped Nd:YVO<sub>4</sub> laser crystal was applied to acquire 2D solid-state laser array which showed the same emitting pattern as the pumping VCSEL. By properly accounting for the thermal focal length of the 2D solid-state laser array, the system enables vertical integration of the VCSEL array with the solid-state laser gain medium. This integration overcomes key limitations of conventional VCSEL arrays, such as low

brightness and large divergence angles, which restrict their use in high-power and long-range optical transmission applications. The integrated 2D solid-state laser array generated a laser bundle consisting of thousands of parallel laser beams. The individual laser beams had good beam qualities, with  $M^2$  values of 1.41 and 1.48 in the X and Y directions, respectively; these results indicated consistent and high-quality beam characteristics across the array. The brightness of the 2D laser array ( $1.27 \text{ kW}\cdot\text{cm}^{-2}\cdot\text{sr}^{-1}$ ) was significantly greater, by three orders of magnitude, than that of the VCSEL array ( $5.9 \text{ W}\cdot\text{cm}^{-2}\cdot\text{sr}^{-1}$ ). Additionally, the performance of the 2D solid-state laser array clearly displayed power scalability with respect to the array size. Common bonding and adhesive techniques for the combined optical components could be employed to assemble the VCSEL array, laser crystal, and output coupler into a fully integrated chip. Furthermore, various modulation components (e.g., Q switching devices) could also be incorporated into the cavity; this facilitates new possibilities for developing compact solid laser arrays with high brightness and peak power. Additionally, the crystal can be actively cooled to enhance heat dissipation and improve system performance under high repetition rates or CW conditions.

**Funding.** National Key Research and Development Program of China (2021YFA1400604, 2021YFB2801400).

**Disclosures.** The authors declare no conflicts of interest.

**Data availability.** Data underlying the results presented in this paper are not publicly available at this time but may be obtained from the authors upon reasonable request

**Supplemental document.** See Supplement 1 for supporting content.

## REFERENCES

- P. Zhao, S. Ragam, Y. J. Ding, *et al.*, *Opt. Lett.* **35**, 3979 (2010).
- Y. Wang, J. A. Holguín-Lerma, M. Vezzoli, *et al.*, *Nat. Photonics* **17**, 338 (2023).
- M. Li, C. Shen, Z. Sun, *et al.*, *Appl. Phys. Rev.* **11**, 021315 (2024).
- L. Wang, C. Zhang, F. Liu, *et al.*, *J. Manuf. Processes* **81**, 562 (2022).
- D. V. Seletskiy, S. D. Melgaard, S. Bigotta, *et al.*, *Nat. Photonics* **4**, 161 (2010).
- Y. Minowa, X. Geng, K. Kokado, *et al.*, *Optica* **9**, 139 (2022).
- T. Steinle, V. Kumar, A. Steinmann, *et al.*, *Opt. Lett.* **40**, 593 (2015).
- Y. Jia and F. Chen, *Chin. Opt. Lett.* **17**, 012302 (2019).
- Y. Zhang, S. Li, X. Du, *et al.*, *Opt. Lett.* **46**, 3641 (2021).
- J. Clark and G. Lanzani, *Nat. Photonics* **4**, 438 (2010).
- K. Hirose, Y. Liang, Y. Kurokawa, *et al.*, *Nat. Photonics* **8**, 406 (2014).
- Z. Chen, A. Sludds, R. Davis, *et al.*, *Nat. Photonics* **17**, 723 (2023).
- L. Goldberg, C. McIntosh, and B. Cole, *Opt. Express* **19**, 4261 (2011).
- P.-C. Di, X.-P. Li, J. Yang, *et al.*, *IEEE Photonics Technol. Lett.* **33**, 395 (2021).
- R. Li, J. Meng, X. Chen, *et al.*, *Chin. J. Lasers* **49**, 1801002 (2022).
- J. Yue, K. Tanaka, G. Hirano, *et al.*, *Nat. Commun.* **13**, 5774 (2022).
- R. Van Leeuwen, B. Xu, Q. Wang, *et al.*, *Proc. SPIE* **10082**, 100820L (2017).
- F. Meng, H. Qu, X. Zhou, *et al.*, *IEEE Photonics Technol. Lett.* **36**, 1489 (2024).